POLITECNICO
MILANO 1863

SCUOLA DI INGEGNERIA INDUSTRIALE
E DELL'INFORMAZIONE

Executive Summary of the Thesis

Geometry optimization of superconducting nanowire single photon detectors (SNSPDs) towards background-free X-ray detection

Laurea Magistrale in Physics Engineering - Ingegneria Fisica

Author: Alessandro Cerioni

Advisor: Prof. Gianluca Valentini

Co-advisor: Stephan Steinhauer Ulirch Vogt Val Zwiller

Academic year: 2021-2022

1. Introduction

Superconducting nanowire single-photon detectors (SNSPDs) exhibit indispensable qualities when dealing with quantum photonics and single-photon oriented applications. Near-unity detection efficiency, up to 98 $\pm$ 0.5% in[1], dark counts as low as 10^{-4} Hz [2], short dead times, time jitters smaller than 3 ps [3], high maximum count rates and large active areas allow them to exceed the performances of many devices used for analogous purposes, such as single-photon avalanche diode (SPAD) and photomultiplier tubes(PMTs). SNSPDs exhibit a wide spectral detection window as well, further increasing their versatility. Indeed, by exploiting both direct and indirect detection mechanisms SNSPD devices can detect photons from mid-infrared (10 μm) [4] up to X-ray range[5]. Nevertheless, SNSPDs response in the X-ray range is still not sufficiently investigated and the detection mechanism still not fully understood. This work is intended to address this need, starting from a precedent work [5] where it is stated that the X-ray detection mechanism is substrate mediated(indirect). The authors argue that X-ray induced production of secondary particles, such as phonon, hot electrons and optical photon contribute to the overall count rate. However, it is stated that SiO_2 (substrate) scintillation should be the major responsible as its luminescence spectrum falls within the visible-infrared range[6]. This thesis project thus investigate the relevance of the substrate (SiO_2) scintillation mechanism in the X-ray detection mechanism of SNSPDs. To do so it is important to fabricate SNSPDs incapable of detecting such photons. Geometry optimization of Niobium titanium nitride (NbTiN) of 12 nm thickness is performed through PHIDL (Python) based programming to fabricate devices with different widths. Such devices have shown to achieve complete suppression of visible-infrared counts (substrate scintillation range), at a wavelength of $\lambda = 850$ nm for widths above 100 nm.

2. Superconductivity key concepts

Superconducting materials are characterised by:
- The critical temperature Tc at which value the material experiences a phase transition from the normal conducting state into the superconducting state.
- The critical current Ic which is the current value over which superconductivity is destroyed.

3. SNSPDs design

To generate designs an innovative programming environment was used: PHIDL. PHIDL is a python-based layouting software, containing many built-in functions associated with geometries and structures related to SNSPDs. This feature makes PHIDL the best program to be used allowing for reduction of coding errors too. The user can design complex 2D geometries for nanolithography and device design [7]. Indeed, Included are functions like snspd(), intended to create SNSPDs using optimized curves, which reduce the problem of superconducting "current crowding". The latter one refers to geometry induced reduction in the critical current of the device. Same reasoning applies for the function optimal.step() [**?**].

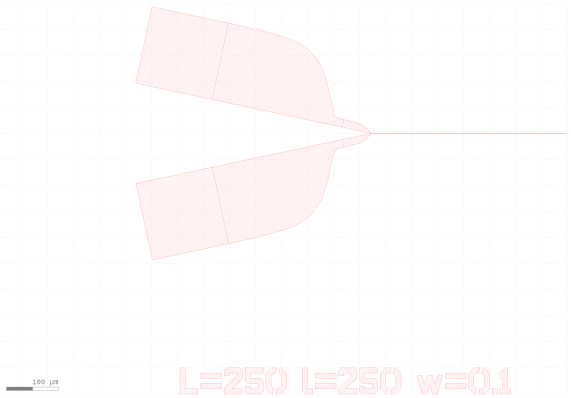

Figure 1: Example Design

4. Detection mechanism (direct)

The process concerning the detection mechanism is schematically reported in Fig.2. The detection process is initiated by a photon impinging on the superconducting device (I) with energy E=hν where, h is the planck constant and ν is the frequency, which, loosing energy, increases locally the temperature of the device to a larger value than bath temperature and Tc, the critical temperature of the superconductor. Upon phonon dissipation, a normal state region is created, referred to as hot-spot (II), which grows up to a maximum dimension (III) and subsequently decays(IV). The bias current, flowing through the device, experiences a normal-conducting domain, resulting in a detectable signal if one of the following conditions are met: either the hot-spot covers the whole cross-sectional area of the device (as schematically shown in the picture (III)), or the current, which is forced to a narrower cross-section, overcomes the critical one. Indeed, if the same current is restricted to flow into a smaller area the current density must increase.

$$I = const = I_b \tag{1}$$

$$I = Jwt \rightarrow J = \frac{I}{wt} \tag{2}$$

As a consequence of the Ohm law and the creation of a normal domain region, an electrical signal is generated detectable with a suitable read-out circuit [8]. Superconductivity is then recovered as the thermal diffusion allows for the operating conditions to be restored.

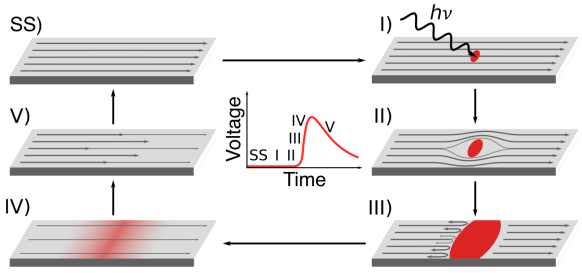

Figure 2: I) photon impingement onto the superconductor device II)hot-spot creation III) hot-spot diffusion covering the whole cross-sectional area IV) decaying of the hot-spot formation V) increase of the bias current flow SS) restored superconducting parameters [3]

5. Indirect detection mechanisms

The expression indirect detection mechanism refers to detection events which are mediated by the substrate. Indeed, as the substrate can also absorb the incoming light, it is possible that secondary emitted particles or back-scattered photons are responsible for the previously described detection mechanism (direct) to take place. As a rule of thumb, the more energetic the incoming light the less relevant is the direct absorption of the thin nanowire and so the direct detection mechanism. For $\lambda = 850$ nm the photon energy is $E = 1.46$ eV while for soft X-ray, as those used in [5], $E = 8$ keV. To estimate the mass photo-absorption coefficient in a NbTiN film, NIST (National institute for standard technology) online calculator is used. The latter one

gives a value of $1.517 * 10^2$ for the mass attenuation coefficient associated to an energy of 7.9 keV, close to the desired one.

$$(\mu/\rho)_{8keV} \propto K\lambda_{8keV}^{2.5/3}Z^4 = 1.517323 * 10^2 cm^2/g, \quad (3)$$

Using for the density of the material $\rho = 6.1 g/cm^3$[5] the computed values correspond to an inverse of the linear attenuation coefficient of ($1/\mu$ is the distance in the material for which the intensity of the incoming beam is reduced of a factor 1/e):

$$1/\mu_{8keV} = 1.08 * 10^{-3} cm = 1.08 * 10^{-5} m, \quad (4)$$

The relevant result is that within a length of $l = 10.8\mu$m the soft x-ray are relevantly absorbed implying that as stated in [5] the main contribution for unity detection efficiency must be ascribable to substrate mediation.

6. Quartz scintillation

At least three arguments suggest that the substrate luminescence might be the major contribution. First SiO_2 X-ray induced scintillation falls within the "blue" range (see Fig.3), approximately around a wavelength of $\lambda = 425 - 440nm$. Secondly, SiO_2 is transparent to such wavelength enhancing the possibility for those photons to reach the superconductor detector [6]. Third, in [5] a nanowire with sufficiently

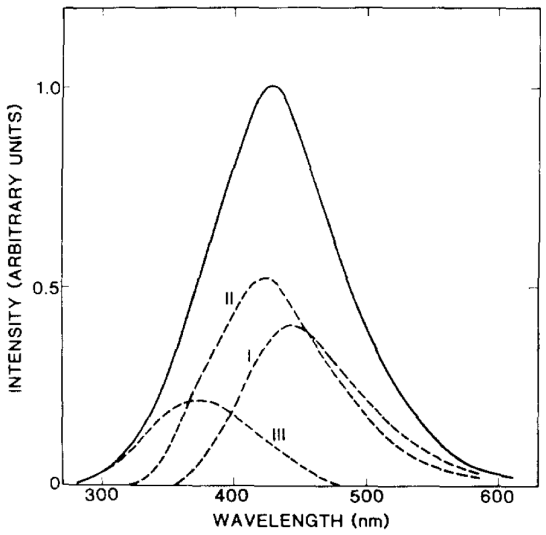

Figure 3: SiO2 X-ray induced luminescence [6]

small cross-sectional area, as we will se with our results, for SiO_2 luminescence direct detection is present.

7. Kinetic inductance and latching mechanism

The kinetic inductance L_k can be regarded as an inertial mass of mobile charges [9]. The large value that the kinetic inductance can assume in a nanowire represents the main contribution to the impedance, since the dc resistance is zero in a superconductor. Its value scales with the length of the device and it is inversely proportional to the cross-sectional area of the nanowire in analogous way to room temperature resistance as reported in the following equations[10]:

$$R_{300K} = \rho_{300K} \int \frac{ds}{A(s)}, \quad (5)$$

$$L_{300K} = l_{300K} \int \frac{ds}{A(s)}, \quad (6)$$

It is relevant for our purpose to understand how the kinetic inductance L_k can be measured. A phenomenological model is proposed in [10],

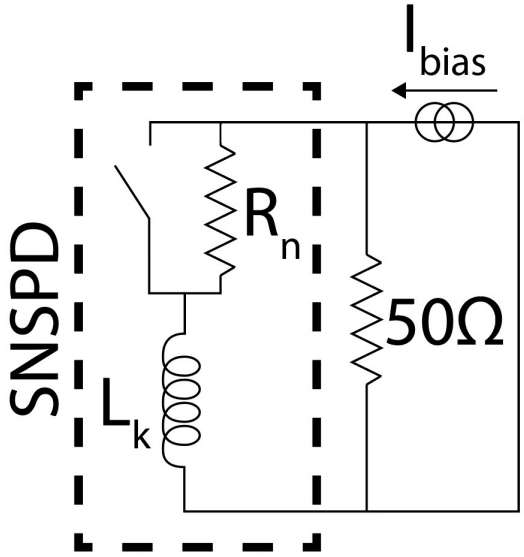

Figure 4: Device scheme

where $R = 50\Omega$ is the output parallel resistance, $R(t)$ is the time dependant resistance of the superconductor and L_K is the kinetic inductance of the nanowire (see Figure4). The presence of a normal-conducting regime (resistance Rn in parallel to the switch), upon hot-spot generation, corresponds to a switch opening,(short circuit equivalent to superconducting state) as a fraction of the bias current is forced to go through a

resistive path. Indeed, while the switch is closed the bias current is utterly directed to the superconducting device, whereas if the switch is open it is necessary to consider the parallel between the generated resistance and the output one. The initial current I_b which flows in the superconducting device starts to decay with a time constant $\tau_{fall} = L_K/[50\Omega + R_n]$ to a final value $I_n = I_b \frac{50\Omega}{[50\Omega+R_n]}$ until the Joule dissipation power $i(t)R_n^2$ is enough reduced, and the superconducting regime is restored (and the switch closes). The current returns then to its original value with a time constant $\tau_{rise} = \frac{L_K}{[50\Omega]}$. From the asymmetry of a generic pulse, as the one reported in Fig.5, it results that $\tau_{rise} >> \tau_{fall}$ and it is therefore possible to conclude that $R_n >> 50\Omega$. Therefore, The value of the kinetic inductance can be extracted from the waveform of the pulse and is proportional to the time constant of the pulse. To allow for fast detection L_k should be small. Nevertheless, in the detection

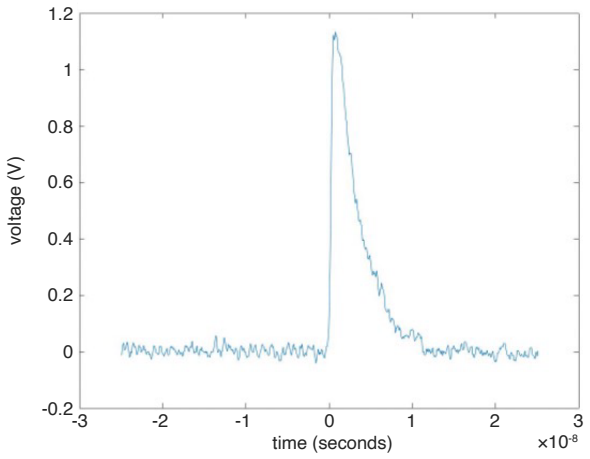

Figure 5: Pulse detected from oscilloscope which decays with a time constant τ_{rise}

process the expansion of a resistive domain due to heating dissipation is counteracted by negative electrothermal feedback from the load resistance. Indeed, the load resistance R_L being much smaller than Rn(t)(see figure4), when the hot-spot reaches the maximum dimension (has demonstrated in previous paragraphs), diverts the current from the device path to the load resistance path. Such decrease, allows the system to reduce heat dissipation and restore the superconducting state. Nevertheless, if L is too short the feedback is stable: I_L, the current flowing through the load path, is sufficiently increased (before on the other wire the superconducting state is restored) to create an equilibrium configuration (latching) in both wire and thus leading to a stable and locked resistive domain, known as a self-heating hotspot [**?**]. For this reason, the desired working mode is the one where the electro-thermal feedback is unstable, allowing for self-recovering of the superconducting state. Therefore L_k should not be too low to avoid latching neither too large, to have a poorly working device.

8. Device characterisation

The fabrication of NbTiN superconducting nanowire single-photon detectors (SNSPDs) is rather challenging due to their crystalline structure. To obtain accurate results, it is important to characterise such devices with their room temperature resistance, critical current value and kinetic inductance values in order to discard non reliable devices.
Typical values of the room temperature resistance are within the 0.1-2 MΩ window. If low values of the room temperature resistance are obtained, it can be inferred that during the fabrication process some resist was not properly removed in some regions within the hairpin, thus leaving the underneath superconducting layer. This will result in a short-circuit. On the contrary, large values of the room temperature resistance (or saturated) are associated with narrower regions along the nanowire, usually referred to as "bottleneck regions".
The critical current value and the overall behavior of the voltage to bias characteristic represent additional criteria. Fig.6 depicts the voltage to bias current behavior of SNSPD devices from the fourth experiment that was carried out. As SNSPDs show no resistance if a current with lower value than the critical one is applied, the voltage to bias current characteristic is a flat function coincident with x-axis. Once the critical current value is reached, a voltage potential difference arises, exhibiting a linear characteristic whose slope depends on the load resistor (in our case 50Ω). The equation relating the critical current to the geometry of the nanowire is:

$$I_c = J_c w t; \tag{7}$$

where J_c is the critical current density, w the

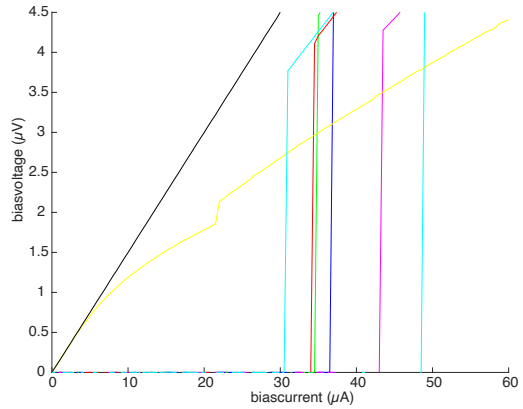

Figure 6: Voltage as a function of critical bias (n4)

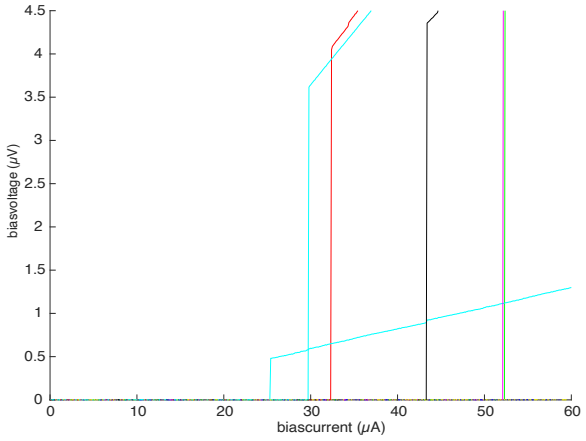

Figure 7: Voltage as a function of critical bias(n3)

width and t the thickness of the device. As both the thickness and Jc are kept constant, the critical current value should vary mainly because of the difference in width. The bias current application window is 0-66 μA. As it can be deducted from Fig.6 the black and yellow lines do not represent a superconducting characteristic. Indeed, both devices show a resistive behavior already from very low values of the bias current. The critical current value, instead, gives information about the status of the device if a comparison is made with critical current values of other devices. From the previous equation it can be inferred that the larger is the width of the device the larger is its critical current value. In addition, devices having the same widths should exhibit similar values for the critical current. A general consideration could be that critical current values lower than expected ones can be associated with narrower widths or with the presence of bottlenecks along the nanowire. An example is reported in Fig.7 where the second cyan characteristic from the left refers to a w=150 nm device (see result section, red squared in table8. Such device shows a relevantly lower value of the critical current, if compared to devices with analogous width green line and purple line and lower resistance value with respect to the device represented by the purple characteristic. This characteristics can arise from a combinations of both short-circuit, responsible for lower resistance, in some region of the meander, and bottlenecks, responsible for lower critical current values and detected counts (see result section). Nevertheless, this should verified a posteriori with the use of SEM imaging.
The kinetic inductance value should fall within a reference window, which typically goes from 50 nH to 200 nH. Indeed, Larger values of the kinetic inductance are associated with small count rates while smaller ones will induce positive electro-thermal feedback (latching of the device), thus not allowing the recovery of the superconducting state upon photon detection. Such value is obtained from and exponential fitting, performed through python, of the pulse waveform.

9. Results

In the previous section the modalities that had been adopted to discard non working devices were argued. The results provided in this section thus only refer to devices which exhibit good parameter values. The results for flood illumination at $\lambda = 850$ nm using NbTiN SNSPDs on SiO_2 substrates are presented. A total of four experiments and 27 devices have been analysed. Just 19 out of 27 devices showed parameters within the suitable ranges. The results counts are summarized in the following table8. The

Widths (nm)	70	100	150	200
Tested devices	3	4	8	4
No counts		3	7	4
1cps < counts < 10 cps		1		
10 cps < counts < 1 kcps				
1 kcps < counts < 10 kcps	3		1	

Figure 8: Scheme of results

only devices showing relevant (>10 kcps) counts

have a width of 70 nm. Just few counts are detected by one device having 100 nm width. We conclude that the width threshold for $\lambda = 850$ nm light detection for NbTiN SNSPDs of 12 nm thickness is close to 100 nm. Nevetheless, an exception is represented by the red squared of the previous figure where a 150 nm device exhibit 9000 cps. As it was discussed in the previous section such device shows weakly inconsistent parameters from the comparison with other device and so it should not be considered entirely reliable.

10. Conclusions and future developments

Results show that the threshold for such wavelength detection is included in the 70-100 nm width range. This result allows us to infer that many fewer detection events will be obtained if an analogous experiment as in [5], i.e., with an X-ray source is performed. If substrate scintillation is found to be the most relevant indirect detection responsible in SNSPDs, by employing the same layout, it will be possible to compare devices showing just direct detection mechanism with devices showing both direct and indirect detection mechanisms. From such comparison it will be possible to quantify the SiO_2 contribution. Future investigations in the X-ray range should look at substrate engineered detectors capable of not only detecting the event but also the energy of the incoming photon.

11. Acknowledgements

I would like to thank my supervisor Stephan Steinhauer without whom this project would not have been possible and my professors Gianluca Valentini, Val Zwiller and Ulrich Vogt for giving me this great opportunity.

References

[1] Sae Woo Nam Richard P. Mirin Dileep V. Reddy, Robert R. Nerem and Varun B. Verma. Superconducting nanowire single-photon detectors with 98% system detection efficiency at 1550nm. *Optica*, 7:1649–1653, 2020.

[2] Hiroki Takesue Hiroyuki Shibata, Kaoru Shimizu and Yasuhiro Tokura. Ultimate low system dark-count rate for superconducting nanowire single-photon detector. *Optics Letters*, 40:3428–3431, 2015.

[3] Johannes W. N. Los Samuel Gyger Ali W. Elshaari Stephan Steinhauer Sander N. Dorenbos Iman Esmaeil Zadeh, J. Chang and Val Zwiller. Superconducting nanowire single-photon detectors: A perspective on evolution, state-of-the-art, future developments, and applications. *Applied Physics letter*, 2021.

[4] V.B. Verma. Single-photon detection in the mid-infrared up to 10 m wavelength using tungsten silicide superconducting nanowire detectors. *APL Photonics*, 2021.

[5] Julien Zichi Iman E. Zadeh Stephan Steinhauer Val Zwiller Artur Branny, Pierre Didier and Ulrich Vogt. X-ray induced secondary particle counting with thin nbtin nanowire superconducting detector. *IEEE TRANSACTIONS ON APPLIED SUPERCONDUCTIVITY*, 2021.

[6] E. E. Kohnke P. J. Alonso, L. E. Halliburton and R. S. Sossoli. X-ray-induced luminescence in crystalline si02. *Journal of Applied Physics*, 1983.

[7] Sonia M. Buckley et al. Adam N. McCaughan, Alexander N. Tait. Phidl: Python-based layout and geometry creation for nanolithography. *J. Vac. Sci. Technol*, 2021.

[8] K.E.GRAY andR.G.WAGNER Alberto-GABUTTI. Granular-aluminum superconducting detector for 6 kev x-rays and 2.2mev beta sources. *NationalInstituteofStandardsandTechnology*, 1989.

[9] R. Meservey and P. M. Tedrow. Measurements of the kinetic inductance of superconducting linear structures. *Journal of Applied Physics*, 2003.

[10] Eric A. Dauler Andrew J. Kerman, Joel K. W. Yang William E. Keicher, Karl K. Berggren G. Gol'tsman, and B. Voronov. Kinetic-inductance-limited reset time of superconducting nanowire photon counters. *APPLIED PHYSICS LETTERS*, 2006.